Towards a Structural Model for the Aluminium Tellurite Glass System

Emma Barney,[1] Nattapol Laorodphan,[2†] Faizani Mohd-Noor,[2‡] Diane Holland,[2] Tom Kemp,[2] Dinu Iuga,[2] and Ray Dupree[2].

[1] *Faculty of Engineering, University of Nottingham, Nottingham, NG7 2RD, UK*
[2] *Physics Department, University of Warwick, Coventry, CV4 7AL, UK*
†*now at Faculty of Science, Maejo University, Chiang Mai, Thailand*
‡*now at Physics Dept., UTM, Johor Bahru, Malaysia*

Supplementary Information

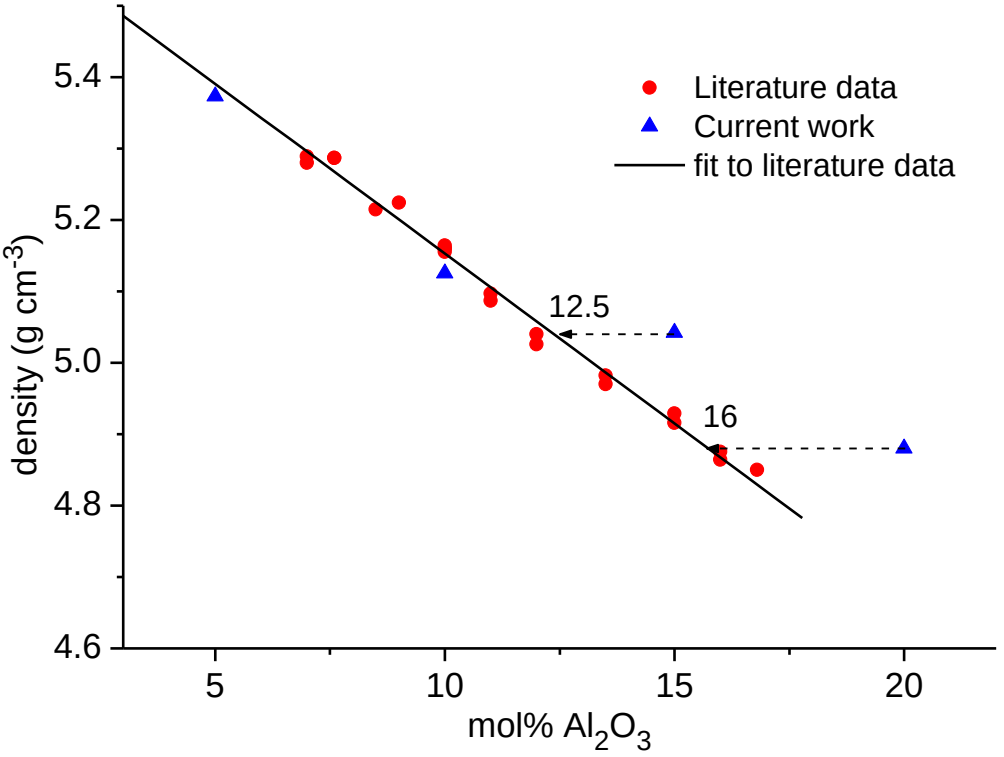

Figure S1: The density values for glasses used in this study are plotted against their nominal Al_2O_3 content and compared with density values reported in the literature.[1-4] Using the straight line fit to the literature data, the compositions of the 15 and 20 mol% samples are revised to 12.5 and 16 mol% as shown. These compositions are used throughout the paper.

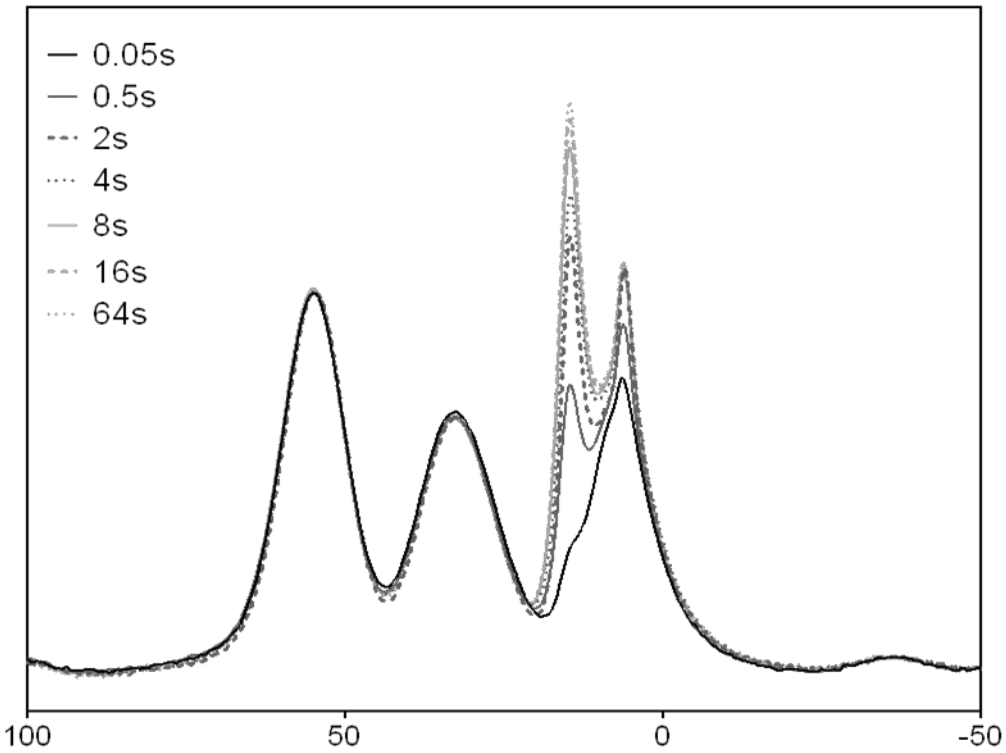

Figure S2: Effect of delay between pulses on ^{27}Al NMR MAS spectra obtained at 20 T from the 16 mol% Al_2O_3 aluminium tellurite sample. The loss of intensity with decreasing pulse delay for the narrow features in the 0 to 20 ppm region means that the relaxation rates for ^{27}Al nuclei in the crystal phase(s) are much longer than for those in the glass. This indicates that the Fe^{3+} dopant ions are rejected from the crystal phase(s) into the residual glass phase.

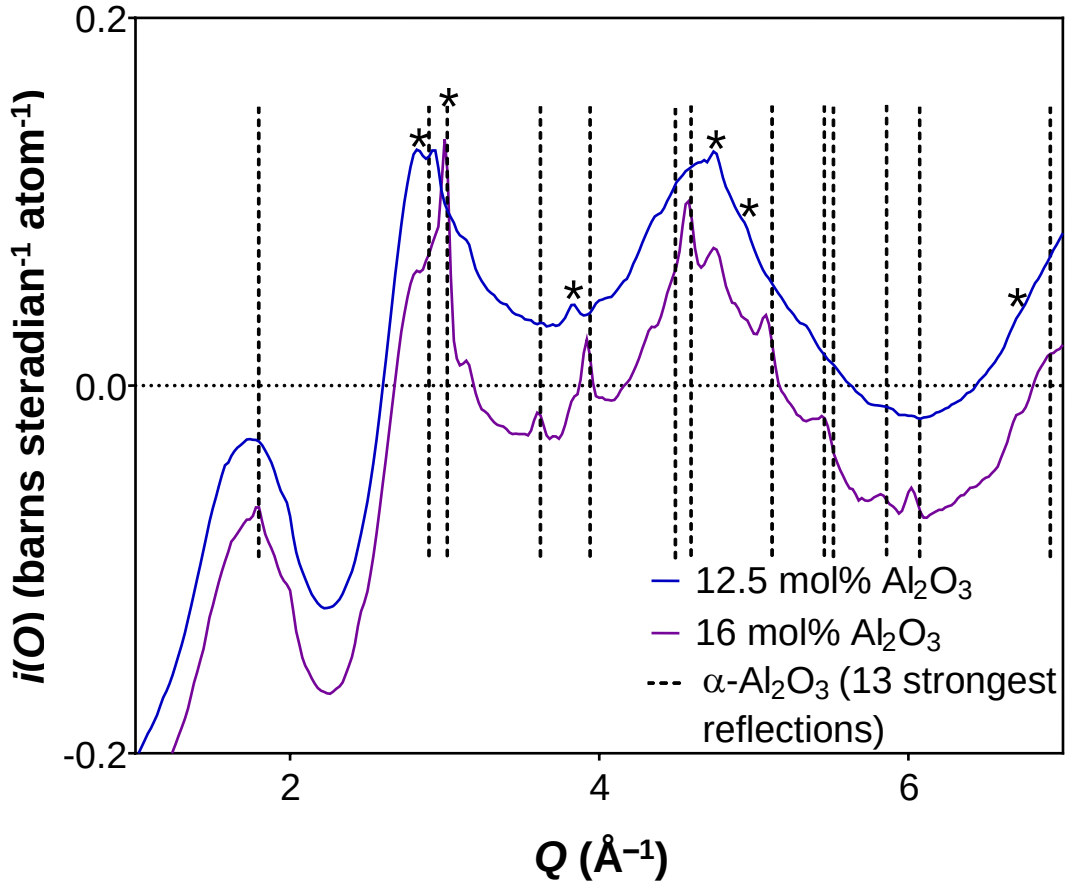

Figure S3: The low Q region (1-7 $Å^{-1}$) of the distinct scattering, $i(Q)$, for the 12.5 and 16 mol% Al_2O_3 samples. The dashed lines show the positions of the most intense Bragg peaks expected for α-Al_2O_3 crystallites. The positions of the six strongest peaks (by X-ray diffraction) for crystalline Al_2TeO_6,[5] are marked with *.

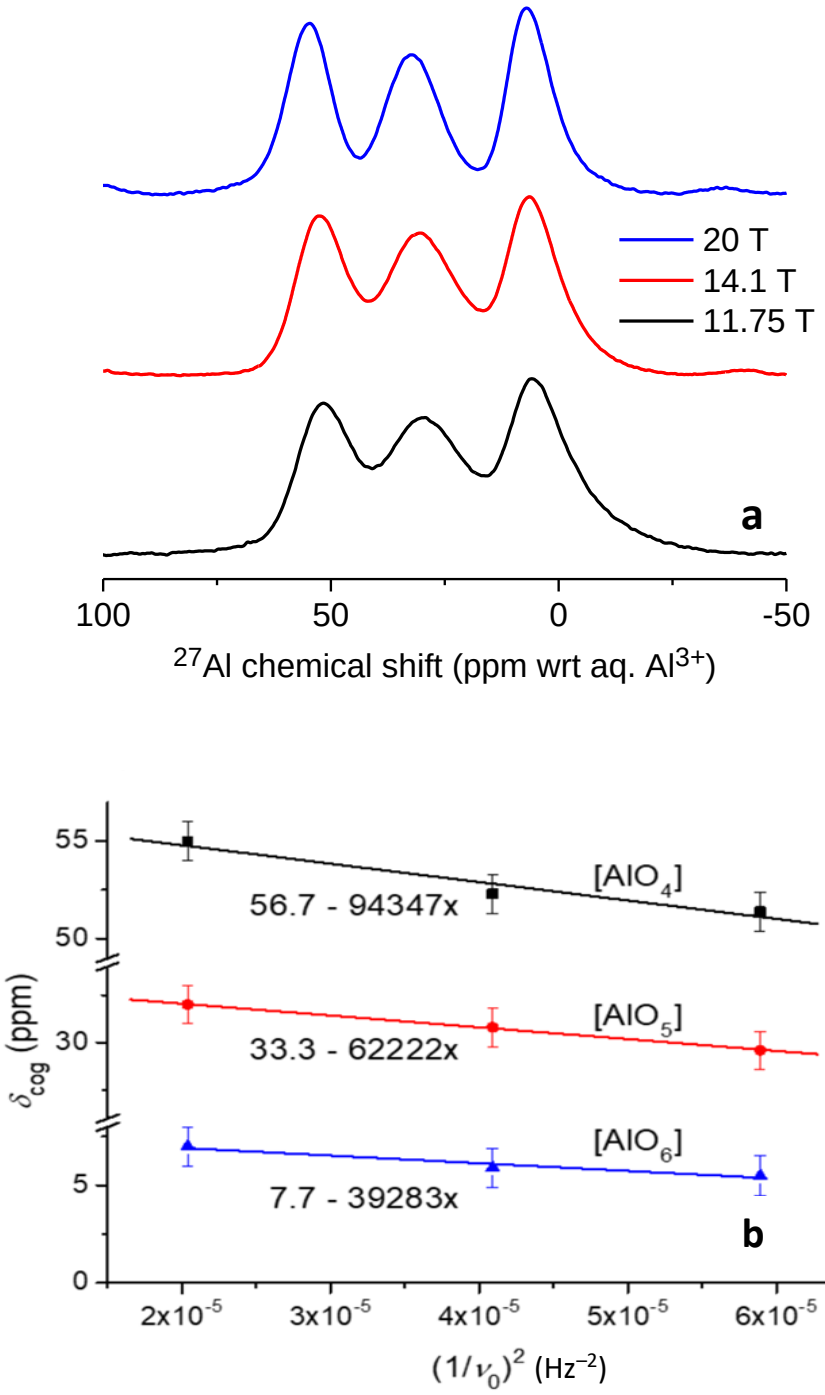

Figure S4: (a) A comparison of the NMR spectra collected at three different fields for the 10 mol% Al_2O_3 aluminium tellurite glass. Peaks are progressively narrowed with increasing field. (b) Plot of $\delta_{cog} = \delta_{iso} - \frac{3}{500}\frac{P_Q^2}{\nu_0^2}$ where δ_{cog} and δ_{iso} are the centre of gravity of the peak and the isotropic shift respectively; ν_0 is the Larmor frequency of ^{27}Al at the given field; and P_Q is the quadrupolar constant ($P_Q^2 = C_Q^2(1 + \eta^2/3)$) which comprises the quadrupole moment C_Q and the asymmetry parameter η.[6]

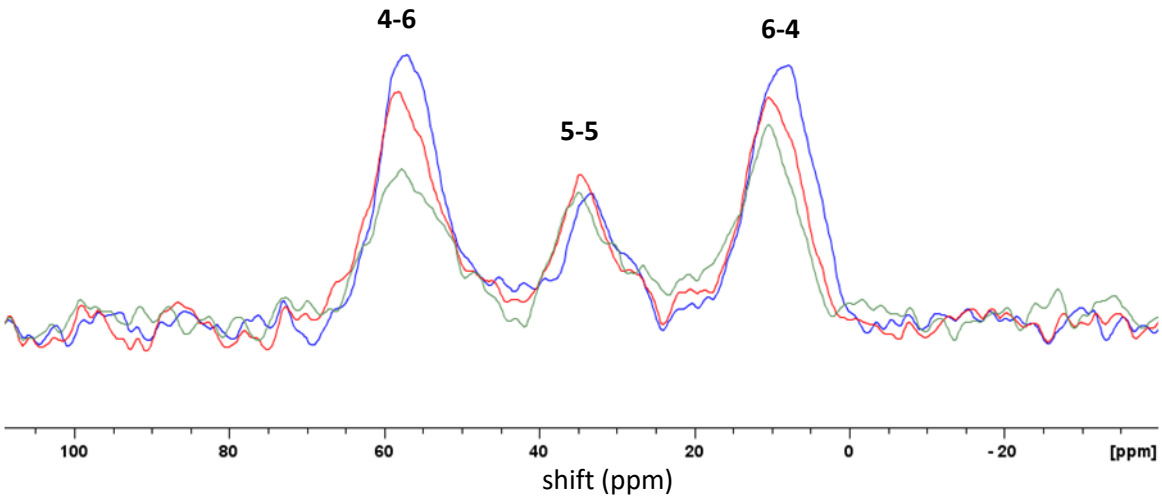

Figure S5: Slices shown are taken through the direct dimension in the DQ spectrum in Figure 6 of the main text. The slices are at 66.3 ppm (blue), 67.7 ppm (red) and 69.5 ppm (green) on the DQ axis and are shown superposed in order to give an indication of the different distributions in intensity of the 4-6, 5-5, and 6-4 peaks. The 5-5 autocorrelation peak is seen quite clearly in the slices whilst being barely visible with the contour levels used in the DQ spectrum of Figure 6 (main text).

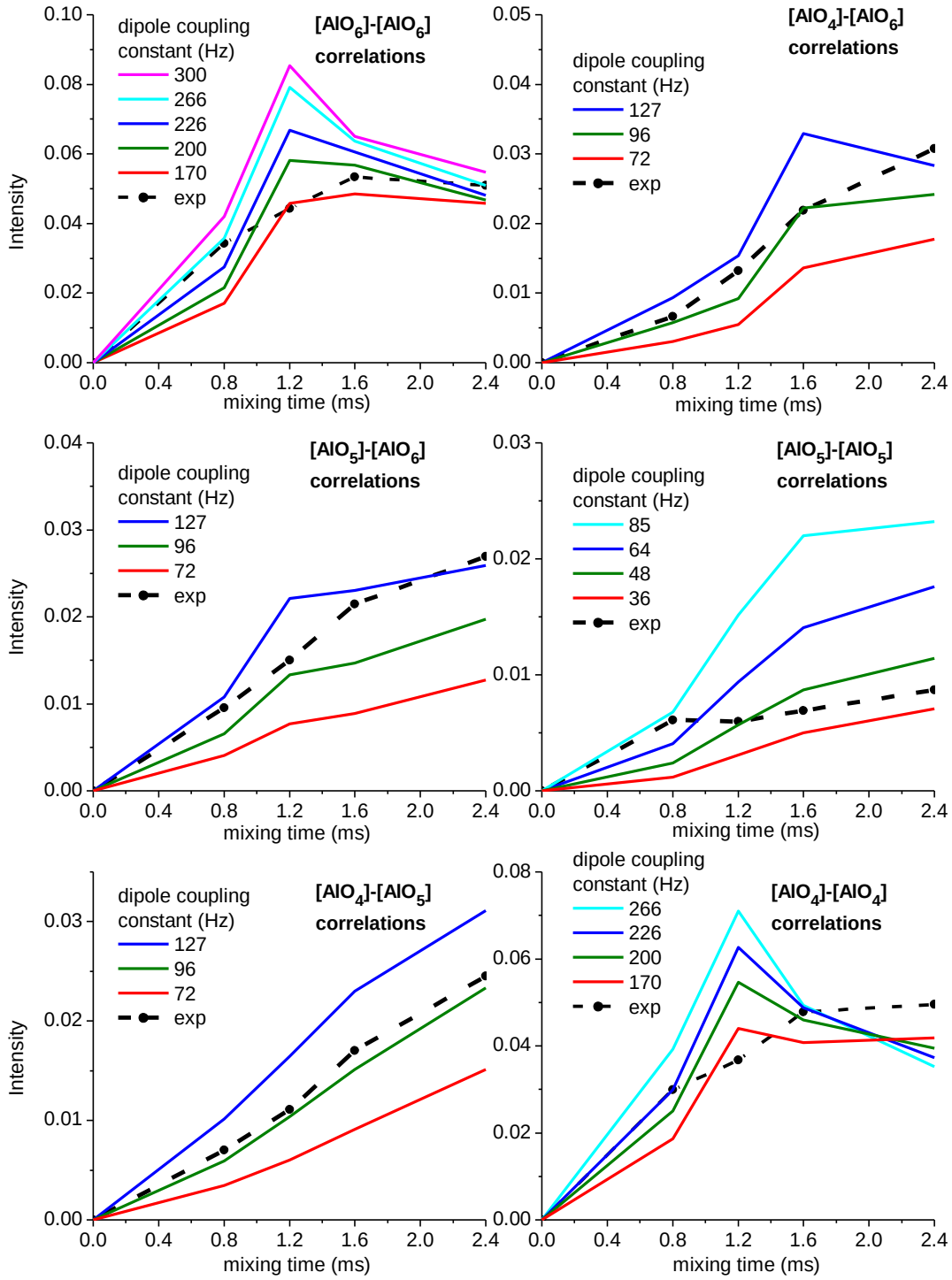

Figure S6: Experimental and simulated[7] build up curves for the DQ MAS NMR experiment. Each simulated build up curve corresponds to a 5% change in distance. For these simulations the shifts were taken from the peak *maxima* e.g. with the [AlO_4] chemical shift being 10630 Hz (48 ppm) from the [AlO_6].

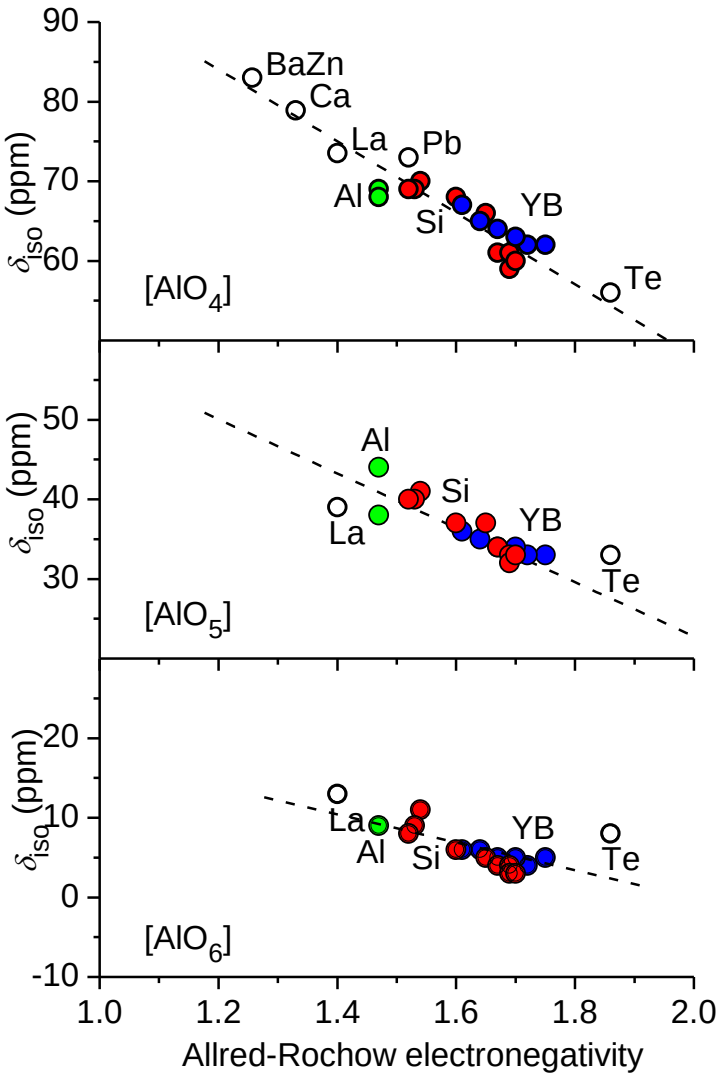

Figure S7: The isotropic shifts, δ_{iso}, reported for the different [AlO_n] species in Al_2O_3 glass and aluminate glasses plotted against the electronegativity values (Allred-Rochow) for Al and the second metal.[8] The electronegativity value for each glass composition is taken as the mean of the contributing cations weighted by their relative abundance. The dashed lines are straight line fits to the data and multiple points of the same colour represent contributions from different reports of the same system or cover the values for the range of compositions in a given report. Whilst most of the glasses included are binary (Al (green),[9-11] Ca,[12] La,[13] Pb,[14] Si (red),[15-16] and Te (this study)), two ternary systems are also included: BaO-ZnO-Al_2O_3 (unpublished results), and Y_2O_3-B_2O_3-Al_2O_3 (blue)[17]. In most cases, the errors in δ_{iso} are within the size of the data points. In the case of the PbO-Al_2O_3 and BaO-ZnO-Al_2O_3 glasses, δ_{iso} has been calculated from the quoted [AlO_4] peak maximum position, δ_{cog}, using $\delta_{cog} = \delta_{iso} - \frac{3}{500}\frac{P_Q^2}{\nu_0^2}$ with ν_0 = 156 MHz and P_Q taken as 5 MHz (typical value in aluminate glasses).[6]

S8: Comments on the microstructure of the glasses used in the study.

The nominally 15 and 20 mol.% Al_2O_3 aluminium tellurite glasses exhibited large scale phase separation into clear and cloudy portions. Neither Kaur et al.[29] or Sakida et al.[27] report cloudy and clear phases for the aluminium tellurite glasses containing 20 and 16 mol% Al_2O_3 respectively[48] although Kaur et al. stated that their sample was only semi-transparent.[29]

Even after separating out the opaque portions, there is still evidence, from both ^{27}Al MAS NMR spectra and neutron diffraction data, of a very small amount of crystallisation (~1-2 % of Al) in the 12.5 mol% Al_2O_3 aluminium tellurite glass used for determining the DQ build-up curves. There is somewhat more crystallisation (~6-8 % of Al) in the 16 mol% glass where two distinct sharp peaks can be seen in the ^{27}Al MAS NMR spectrum, shown in Figure 4 (main text). One peak is at ~15 ppm, the expected position of a peak arising from α-Al_2O_3[6], and similar to a peak observed by Kaur et al. for a nominally 20 mol% Al_2O_3 aluminium tellurite glass.[18] The second sharp feature in the ^{27}Al MAS NMR spectra, present in both the 12.5 and 16 mol% Al_2O_3 aluminium tellurite glasses, is at ~6 ppm. We assign this chemical shift to the second, unknown, crystal phase. The low Q region (1-10 Å^{-1}) of the distinct scattering data for the 12.5 and 16 mol% Al_2O_3 samples, plotted in Figure S3 of supplementary information (SI), also shows evidence of crystallisation, exhibiting a number of Bragg peaks. Not all the peaks present in the glass modified with 16 mol% Al_2O_3 are evident in the distinct scattering for the 12.5 mol% Al_2O_3 aluminium tellurite glass confirming an additional crystal phase is present in the 16 mol% Al_2O_3 aluminium tellurite. The expected positions for the 13 most intense Bragg peaks arising from α-Al_2O_3 crystallites are shown with the experimental data as dotted lines. These lines are a poor match to the peaks observed in the distinct scattering from the glass containing 12.5 mol% Al_2O_3, but match well with the most intense peaks in the distinct scattering from the glass containing 16 mol% Al_2O_3, confirming the assignment to Al_2O_3 of the peak at ~15 ppm in the ^{27}Al MAS NMR spectrum for this glass. There are no reported aluminium tellurite crystal structures, but there is one report of an XRD powder pattern for the aluminium *tellurate* Al_2TeO_6 containing Te(VI).[5] The positions of the six strongest peaks observed in the X-ray pattern for this crystal phase are each denoted by an asterisk in Figure S3 in SI. The position of each asterisk has reasonably good agreement with the positions of unidentified peaks in $i(Q)$ for the 12.5 and 16 mol% Al_2O_3 aluminium tellurite glasses. Therefore, the second crystal phase is tentatively assigned to be Al_2TeO_6. The structure of this crystal phase is unknown, but the peak at ~6 ppm in the ^{27}Al MAS NMR spectrum indicates that the aluminium atoms adopt [AlO_6] environments. An investigation of the Al_2O_3-TeO_2-O system by Sestak[19] indicates that it is the oxidation of Te(IV) to Te(VI) in air which limits 100% glass formation to about 10 mol% Al_2O_3 as a consequence of the crystallisation of Al_2TeO_6 – this does not occur in vacuum. Oxidation has been reported by Su *et al*. as commencing above approximately 620 °C for a 1:1 sample.[5] This is below the 800 °C melting temperature used for preparing the glasses in this study and can explain the presence of the crystal phases in the nominal 15 and 20 mol% Al_2O_3 samples.

SEM/EDX and also micro-Raman have also been used to study the glass microstructure. However, Figure S8a in SI shows that, for the 10 % Al_2O_3 sample, the only features resolvable by SEM (~0.2 μm

resolution) are a few, widely dispersed, faceted crystallites of dimension 2 to 5 μm. There is insufficient crystal phase at this composition to be detected by neutron or X-ray diffraction but the quantities increase with Al_2O_3 (12.5 % Al_2O_3 Figure S8b) and can then be observed in diffraction patterns and in ^{27}Al NMR spectra as reported above. The micro-Raman spectra (Figure S8c in SI) from each sample are unchanged between different locations within a given glass but do change systematically between samples with different Al_2O_3 content. From this we can conclude that the glass-in-glass phase separation in these samples cannot be resolved by SEM or by micro-Raman (~0.5 μm) consistent with their transparency. The largest Al_2O_3 content, ~40 mol%, determined by SEM/EDX for the crystal phase is significantly less than the 50 mol% expected for the $Al_2Te(VI)O_6$ phase identified by XRD. However, the crystals observed by SEM are of similar size to the excitation volume of the electron beam (~1 micron) so the EDX analysed composition is distorted by contributions from the surrounding glass phase of higher TeO_2 content and which probably account for the underestimate. This would be consistent with the observed diffraction peaks in the neutron data for the 12.5 and 16 % samples. This phase contains Te in its +6 oxidation state and a resonance due to Te(VI) in the ^{125}Te NMR spectrum would be expected at ~+700 ppm (Fig S8d). However, the crystals are of such low abundance that the corresponding static ^{125}Te NMR peak cannot be resolved from the background noise and the tail of the Te(IV) peak.

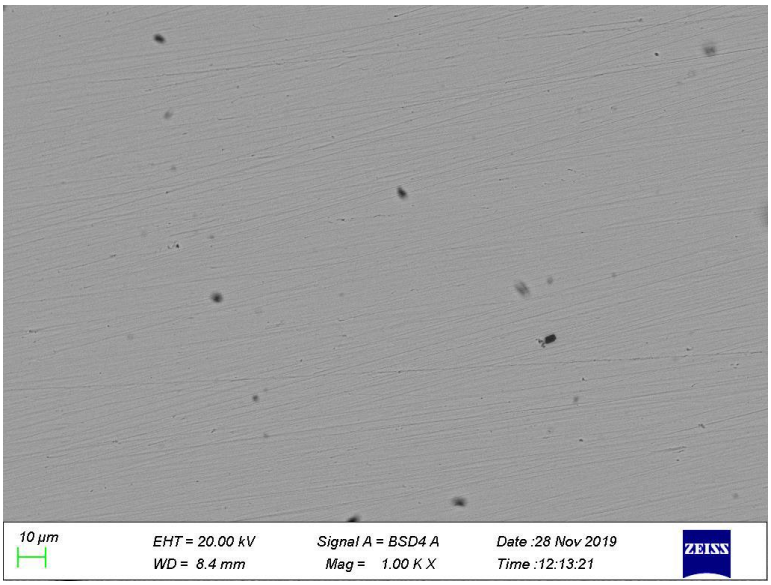

Figure S8a: Typical SEM image of 10 mol% Al_2O_3 glass.

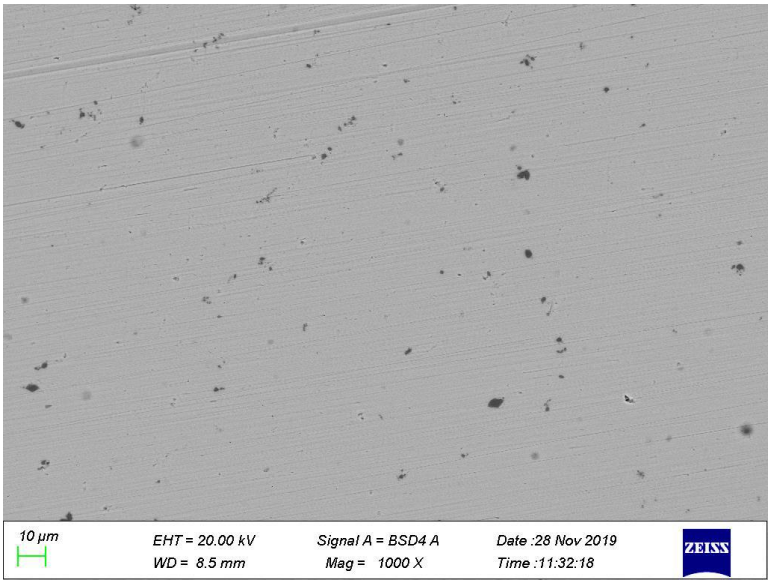

Figure S8b: Typical SEM image of 12.5 mol% Al_2O_3 glass.

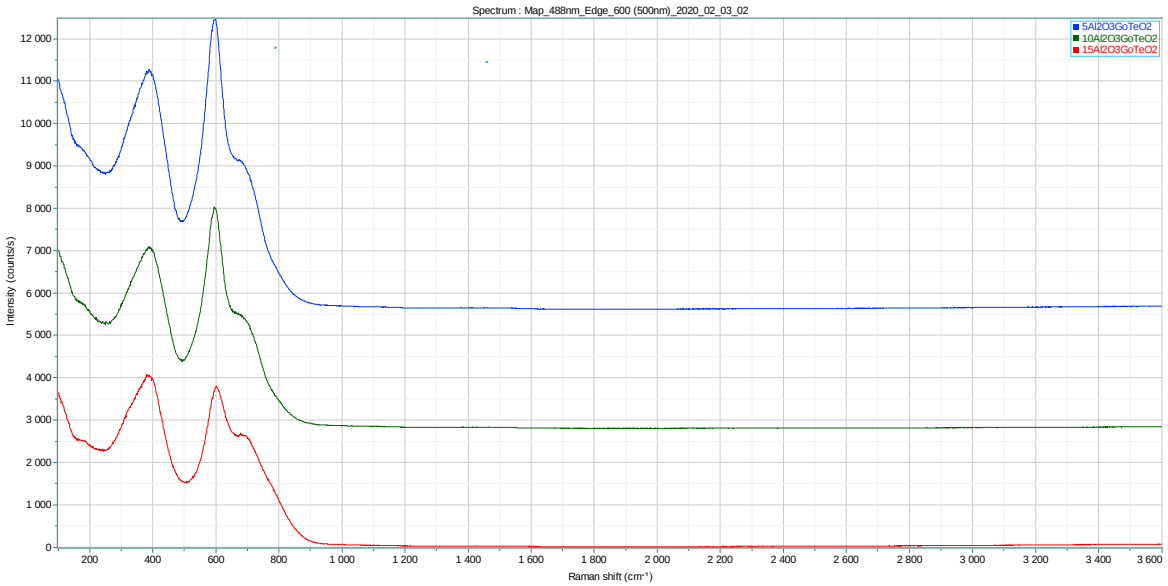

Figure S8c: Micro-Raman spectra from 5 (blue), 10 (green) and 12.5 (red) mol% Al_2O_3 glasses.

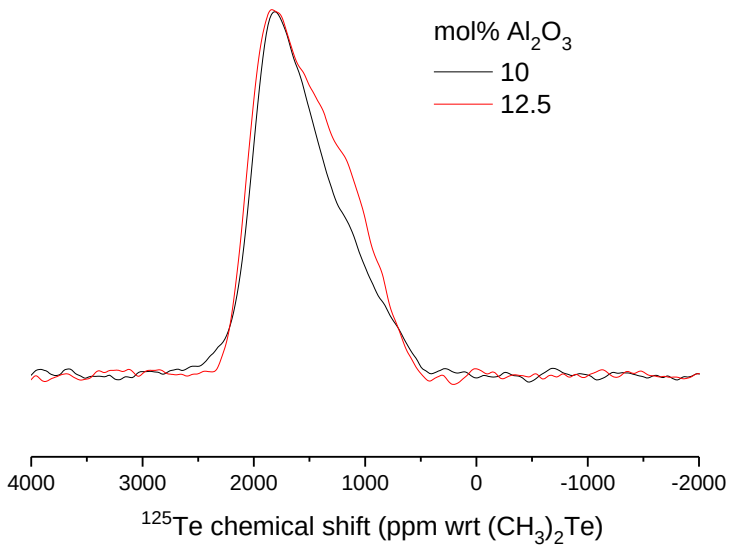

Figure S8d: Overlay of ^{125}Te static NMR spectra of 10 mol% Al_2O_3 (black) and 12.5 mol% Al_2O_3 (red) glasses (normalised to maximum intensity). Any signal due to Te(VI) would be expected at ~700 ppm.

References

1. Burger, H.; Vogel, W.; Kozhukharov, V., IR Transmission and Properties of Glasses in the TeO_2- R_NO_M,R_NX_M,$R_N(SO_4)_M$,$R_N(PO_3)_M$ and B_2O_3 Systems. *Infrared Phys.* **1985**, *25*, 395-409.
2. Takebe, H.; Fujino, S.; Morinaga, K., Refractive-index Dispersion of Tellurite Glasses in the Region from 0.40 to 1.71 μm. *J. Am. Ceram. Soc.* **1994**, *77*, 2455-2457.
3. Kozhukharov, V.; Burger, H.; Neov, S., Glassforming, Properties and Structure of Halide Tellurite Glasses. *Mater. Sci. Forum* **1991**, *67-68*, 143-148.
4. Inaba, S.; Oda, S.; Morinaga, K., Heat Capacity of Oxide Glasses at High Temperature Region. *J. Non-Cryst. Solids* **2003**, *325*, 258-266.
5. Su, X. M.; Wu, A. Y.; Vilarinho, P. M., Al_2TeO_6: Mechanism of Phase Formation and Dielectric Properties. *Scr. Mater.* **2012**, *67*, 927-930.
6. Mackenzie, K. J. D.; Smith, M. E., *Multinuclear Solid-state NMR of Inorganic Materials*, 1st ed.; Pergamon: Oxford, 2002; Vol. 6, p 702.
7. Bak, M.; Rasmussen, J. T.; Nielsen, N. C., SIMPSON: A General Simulation Program for Solid-state NMR Spectroscopy. *J. Magn. Reson.* **2000**, *147*, 296-330.
8. Winter, M., Source: WebElements [http://www.webelements.com/].
9. Dupree, R.; Farnan, I.; Forty, A. J.; Elmashri, S.; Bottyan, L., A MAS NMR-Study of the Structure of Amorphous Alumina Films. *J. Phys.* **1985**, *46*, 113-117.
10. Lee, S. K.; Ryu, S., Probing of Triply Coordinated Oxygen in Amorphous Al_2O_3. *J. Phys. Chem. Lett.* **2018**, *9*, 150-156.
11. Cui, J., et al., Aluminum Oxide Thin Films from Aqueous Solutions: Insights from Solid-State NMR and Dielectric Response. *Chem. Mater.* **2018**, *30*, 7456-7463.
12. Amin, S. A.; Leinenweber, K.; Benmore, C. J.; Weber, R.; Yarger, J. L., Characterizing Pressure-Induced Coordination Changes in $CaAl_2O_4$ Glass Using Al-27 NMR. *J. Phys. Chem. C* **2012**, *116*, 2068-2073.
13. Lo, A. Y. H.; Eden, M., Efficient Symmetry-based Homonuclear Dipolar Recoupling of Quadrupolar Spins: Double-quantum NMR Correlations in Amorphous Solids. *Phys. Chem. Chem. Phys.* **2008**, *10*, 6635-6644.
14. Barney, E. R.; Hannon, A. C.; Holland, D.; Winslow, D.; Rijal, B.; Affatigato, M.; Feller, S. A., Structural Studies of Lead Aluminate Glasses. *J. Non-Cryst. Solids* **2007**, *353*, 1741-1747.
15. Weber, R.; Sen, S.; Youngman, R. E.; Hart, R. T.; Benmore, C. J., Structure of High Alumina Content Al_2O_3-SiO_2 Composition Glasses. *J. Phys. Chem. B* **2008**, *112*, 16726-16733.
16. Ren, J. J.; Zhang, L.; Eckert, H., Medium-Range Order in Sol-Gel Prepared Al_2O_3-SiO_2 Glasses: New Results from Solid-State NMR. *J. Phys. Chem. C* **2014**, *118*, 4906-4917.
17. Deters, H.; de Lima, J. F.; Magon, C. J.; de Camargo, A. S. S.; Eckert, H., Structural Models for Yttrium Aluminium Borate Laser Glasses: NMR and EPR Studies of the System $(Y_2O_3)(0.2)$-$(Al_2O_3)(x)$-$(B_2O_3)(0.8-x)$. *Phys. Chem. Chem. Phys.* **2011**, *13*, 16071-16083.
18. Kaur, A.; Khanna, A.; Gonzalez-Barriuso, M.; Gonzalez, F.; Chen, B. H., Short-range Structure and Thermal Properties of Alumino-Tellurite Glasses. *J. Non-Cryst. Solids* **2017**, *470*, 14-18.
19. Sestak, V. Z. Investigation of the system Al_2O_3-TeO_2-O_2. Masters Thesis, University of Missouri--Rolla, 1970.